

# A Phantom-free Method to Image the Ultrasound Attenuation Coefficient Slope Using Decorrelated Compounding in Synthetic Transmit Aperture Ultrasound Imaging

Khalid Abdalla, Na Zhao, and Yuan Xu, *Member, IEEE*

**Abstract**—We propose a method that employs the decorrelated compounding method [Zhao2022DCjasael] to reduce speckle variation in ultrasound images for estimating the attenuation coefficient in Synthetic Transmit Aperture (STA) imaging. The transducer bandwidth was divided into several overlapping sub-bands. Each sub-band's RF signals are processed by using the decorrelated compounding to reconstruct an image, the derivative of which over depth yields the attenuation coefficient of each sub-band. The attenuation coefficient slope (ACS) was estimated by taking the derivative of the attenuation coefficient over frequency. This method was validated through numerical simulations and empirical experiments involving a tissue-mimicking commercial phantom and a two-layered phantom composed of beef over the commercial phantom. For all data sets, an ROI with a 1 cm window size was utilized to estimate attenuation. Simulations with five phantoms preset at 0.7 dB/cm.MHz resulted in an average attenuation coefficient of 0.73. The experimental phantom was similarly set at 0.7 dB/cm.MHz, and yielded an attenuation coefficient of 0.72. In the beef-phantom composite, the average ACS was 1.1 dB/cm-MHz for beef and  $0.68 \pm 0.03$  dB/cm-MHz for the phantom. The results highlight the effectiveness of this approach for estimating the attenuation coefficient slope. The synthetic aperture technique combined with decorrelated compounding offers benefits over traditional B-mode imaging in terms of phantom-free feature, good spatial resolution, and accurate quantification of tissue properties due to the high SNR and minimum-diffraction effect in ultrasound images. The estimated attenuation coefficient can be used as a biomarker for diagnosis, treatment monitoring, and other quantitative ultrasound methods like particle size estimation.

**Index Terms**—Attenuation coefficient, Image reconstruction, Ultrasonic imaging, Synthetic Transmit Aperture

## I. INTRODUCTION

Ultrasound imaging plays a vital role in medical diagnostics, providing real-time visualization of anatomical structures and assisting in detecting and characterizing various diseases [1]. A fundamental parameter in ultrasound imaging is attenuation coefficient slope (ACS), which provides valuable information about tissue composition and can aid in diagnosing and monitoring pathological conditions [2]. ACS is instrumental in assessing liver diseases, like fibrosis and steatosis, offering insights into tissue damage and assisting in treatment planning [3]. It has also been applied in breast imaging to distinguish between benign and malignant lesions, thereby enhancing diagnostic accuracy and reducing unnecessary biopsies [4].

This work was supported in part by Natural Sciences and Engineering Research Council of Canada (NSERC), Canada Foundation for Innovation (CFI), and Toronto Metropolitan University.

Khalid Abdalla is with Department of Physics, Toronto Metropolitan University, 350 Victoria Street, Toronto, Ontario, Canada. (e-mail: k1abdalla@torontomu.ca).

Zhao Na is with Department of Physics, Toronto Metropolitan University, 350 Victoria Street, Toronto, Ontario, Canada. (e-mail: na.zhao@torontomu.ca).

Yuan Xu is with Department of Physics, Toronto Metropolitan University, 350 Victoria Street, Toronto, Ontario, Canada. (e-mail: yxu@torontomu.ca).

ACS has shown promise in monitoring therapy response, characterizing tumors, and assessing the progression of diseases in organs like the kidney and prostate [5, 6]. It also plays a role in other Quantitative Ultrasound (QUS) methods, like particle size estimation [1, 7]. Consequently, accurate ACS estimation is paramount for a multitude of clinical applications in ultrasound imaging.

Several frequency-domain techniques have been developed to estimate the ultrasound attenuation coefficient. For instance, the spectral-shift method estimates ACS by measuring the downshift in the center frequency of the radio-frequency signals with depth. This method operates on the assumption that the spectral shape of the RF envelope resembles a Gaussian curve [8, 9]. Conversely, reference phantom methods, which include the spectra difference method, spectra log difference method, and the hybrid method, use phantoms with known ACS and scattering properties to account for the frequency and depth-dependent system effects. These system effects typically include the diffraction effect [term  $D(f, z)$  in Eq. 1], which represents the effect of the ultrasound beam converging and diverging on the attenuation estimation in B-mode imaging. Since the diffraction effect depends on both the frequency and depth, it can significantly impact the quality and interpretability of ultrasound attenuation estimation [10–12]. In the

pursuit of improving the estimation accuracy while preserving spatial resolution, recent studies have explored alternative approaches. One such approach involves incorporating regularization techniques with a spatial prior, which has shown promise in enhancing both the precision and resolution of quantitative ultrasound (QUS) estimation in homogeneous regions [12–14]. Spatial and frequency compounding techniques were used to enhance the precision of quantitative ultrasound parameters and considerably decrease the variance for ACS [8, 15–17]. However, the clinical implementation of the reference-phantom method has been slow, hindered by the need to scan a well-calibrated reference phantom with the same clinical equipment and settings used to acquire data from the patient [18].

Ping et al. [19] introduced the reference frequency method that normalizes the system effects by calculating the ratio between the power spectra of each frequency and its adjacent frequency to estimate ACS without a well-calibrated phantom. Despite its effectiveness, the requirement for a predefined frequency range and the use of a large analysis window of 2.5 cm length can limit its feasibility in detecting lesions and other abnormalities within heterogeneous media. Rafati[20] applied the reference frequency method to homogeneous and heterogeneous phantoms with parametric regularization to reduce image artifacts. Such limitations emphasize the continuous need for methodological advancements in this field, especially as the complexity and variability of clinical scenarios increase.

All the above methods used B-mode imaging, which relies on a single transmit-receive aperture. The attenuation coefficient slope was estimated from each individual A-line and averaged over many A-lines. The Synthetic Transmit Aperture (STA) has emerged as a promising approach to address the limitations of conventional B-mode ultrasound imaging [21]. Unlike B-mode imaging which focuses at one point, the Synthetic Transmit Aperture (STA) image can be optimally focused at every point at a high frame rate. In synthetic aperture images, transducer elements transmit an unfocused spherical wave covering the entire image, one element at a time, while all or a part of the aperture samples the received signals. If the nonlinear effect is ignored, the STA data set has more information than B-mode one because B-mode data can be synthesized from STA data, while the process to recover STA data from B-mode one is subject to introducing noise in principle and needs regularization. Furthermore, synthetic aperture techniques can effectively suppress speckle noise, improve lateral resolution, and mitigate the impact of tissue heterogeneity [22–24]. These advantages make the synthetic aperture technique a valuable tool for ACS estimation in clinical practice.

Recently, we developed a method to reduce the image intensity fluctuation due to speckles in the STA images. We applied a decorrelation procedure to the traditional compounding method in STA. The decorrelated compounding (DC) method substantially reduced the speckle variation compared to the conventional B-mode imaging [22, 25]. In this work, we propose to use this method for robust ACS estimation in the STA technique. Since DC reduces the speckle variation significantly, a smaller window size can be used to estimate

ACS. Consequently, the image resolution is better than the B-mode based attenuation estimation method. In addition, the image is optimally focused at every pixel in STA, so the diffraction effect in ACS estimation can be minimized, which makes the reference phantom unnecessary. In summary, the proposed method has the benefits of reference-phantom-free feature, higher spatial resolution, and accurate quantification of tissue properties due to the high SNR and minimum diffraction in ultrasound images.

The structure of this paper is as follows: Section 2 provides an introduction to the modeling of backscattered ultrasound signals and presents the theoretical foundation for ACS estimation. Additionally, the experimental setups, including simulations and tissue-mimicking phantoms, are explained. In Section 3, the results from both the simulation and phantom studies are presented. Section 4 focuses on evaluating the performance of ACS estimation in synthetic aperture imaging. This section also discusses potential future research directions. Finally, Section 5 concludes the paper.

## II. METHOD

### A. Theory

In approximation, the pressure amplitude of the backscattered signals obtained from a region of interest (ROI) at depth  $z$  from the transducer with frequency  $f$  can be modeled as [10, 26].

$$S(f, z) = P(f) \cdot D(f, z) \cdot BSC(f, z) \cdot A(f, z) \quad (1)$$

$P(f)$  is the transducer response function at frequency  $f$ ,  $D(f, z)$  is the diffraction effect,  $BSC(f, z)$  is the backscatter coefficient within the gated window,  $A(f, z)$  represent the total attenuation along the propagation path from the transducer to the beginning of the ROI. For most tissue,  $A(f, z)$  can be approximated as [27].

$$A(f, z) = \exp(-2\mu(f)z) \quad (2)$$

where  $\mu(f)$  (dB/cm.MHz) is the frequency-dependent attenuation coefficient. Notice that we have a factor of 2 in the above equation because the pressure amplitude rather than the power spectrum or intensity is studied here. For biological tissues, it is usually assumed  $\mu(f) = \alpha f$  for simplicity, where  $\alpha$  is the attenuation coefficient slope of the ROI in dB/cm.MHz.

In this paper, we assume  $BSC(f, z)$  doesn't change with depth within a homogeneous region of interest (ROI) used to estimate attenuation. This assumption limits our methods to uniform regions of the sample. This limitation will be addressed in the discussion section. In STA, the image is optimally focused at all pixels. Therefore,  $D(f, z)$  can be assumed as a constant in the ROI. Taking the natural logarithm of equation (1), the attenuation coefficient ( $\mu$ ) can be expressed as the derivative of pressure amplitude over the depth ( $z$ ) direction,

$$\frac{\partial \ln(S(f, z))}{\partial z} = -2\mu. \quad (3)$$

To effectively estimate the attenuation, a ROI window of size 1 cm x 1 cm, centered at depth  $z$ , is employed. This analysis window is specifically designed to ensure both precision

and uniformity in evaluation. Within this window, there are 50 vertical lines, each spaced 0.22 mm apart laterally. To enhance the signal-to-noise ratio of the estimated ACS, results from the central 30 acoustic lines within this window are averaged. Notably, to ensure consistency across the analyses, a substantial overlap of 98% is maintained for all selected analysis windows. To implement the derivative over the depth and frequency, linear regression was applied to the ROI to obtain  $\mu$  first, and then  $\alpha$ , the attenuation coefficient slope. In order to mitigate potential errors arising from the nonlinearity of frequency-dependent attenuation in the phantoms, the fitting for the attenuation coefficient slope was restricted to a frequency range of 2 -5 MHz [28]. It is important to note that these window dimensions and overlaps were kept constant for all the results presented in this study.

### B. Decorrelated compounding in STA

The method of Decorrelated Compounding in Synthetic Transmit Aperture (DC in STA) [29] was adapted to obtain the pressure amplitude of the backscattered signals  $S(f, z)$ . The DC in STA can effectively reduce the speckle variations, improving attenuation coefficient estimation accuracy. The aperture domain and frequency spectrum of RF data were divided into sub-aperture and sub-band signals using a translating and overlapping filter. The Delay-and-Sum operator was applied to these sub-aperture and sub-band signals, reconstructing a series of sub-images. The eigenvectors and eigenvalues of the covariance matrix for the sub-images were used to remove the correlation among sub-images before incoherent compounding in [29]. Theoretically, the averaged variance of  $N$  uncorrelated sub-images can be reduced by a factor of  $\sqrt{N}$ . Therefore, the decorrelation procedure can improve the speckle variance reduction performance by removing the correlations among sub-images compared to the traditional incoherent compounding.

In this paper, we only applied decorrelated compounding to the sub-images within the same temporal sub-band spectrum to obtain the attenuation coefficient corresponding to the sub-band frequency. The compounding result for each sub-band is denoted as the pressure amplitude  $S(f, z)$ , where  $f$  is the central frequency of the selected sub-band. We used a sub-aperture of 32 elements, a quarter of the full array probe, to reconstruct one sub-image. The step size between the two adjacent sub-apertures was 16 elements. These configurations were the same in the transmission and receiving apertures, resulting in 7 sub-apertures along the transmission and receiving dimensions. The total number of sub-apertures/sub-images for one sub-band was  $N_{SC} = 49$ . Therefore, the speckle SNR is expected to improve by 7 times. The bandwidth of a sub-band and the step size for the adjacent two sub-bands were 0.6 MHz and 0.3 MHz, respectively.

### C. Simulation and experiment configurations

The method used to estimate the frequency-dependent attenuation coefficient was tested using the simulated and experimental RF data. For simulation model, The Field II Simulation package was employed to generate simulated raw RF data

from phantoms that generate speckles [30]. A phased array transducer consisting of 128 elements, with a width of 2.79 cm and operating at a nominal frequency of 3.47 MHz, was positioned 3 mm above the phantoms. The probe configuration used in the simulation matched that of the experimental probe. In the Field II program, a scattering medium with an ACS  $\alpha = 0.7$  dB/cm-MHz and sound wave velocity of 1540 m/s were adopted. A complete set of synthetic aperture data was sampled at a rate of 13.88 MHz. The dimensions of the reconstructed image were 4 cm in the axial direction and 2.79 cm in the lateral direction. In order to investigate the fluctuation characteristics of the backscattered spectrum signals, five independent scattering mediums were used to generate the backscattered signals. The attenuation coefficient slope (dB/cm-MHz) was measured for each simulated phantom, yielding five unique values representing the attenuating properties of these phantoms. To obtain a more accurate and reliable estimate, the average attenuation coefficient slope across these five simulations was then calculated. In addition, the standard deviation (STD) was computed, providing a measure of the variance in the attenuation coefficients of the different phantoms.

We used the Verasonics Vantage Research Platform (Verasonics Inc., Kirkland, WA) to acquire the experimental RF data in a model 040GSE (CIRS Inc., Norfolk, VA) phantom. The attenuation coefficient in the imaged areas were  $\alpha = 0.7$  and 0.5 dB/cm-MHz and the acoustic wave velocity was 1540 m/s according to the specifications provided by the manufacturer. The STA data were processed by applying the delay-and-sum beamforming to reconstruct the sub-images from the sub-band and sub-aperture RF signals. Then the decorrelated compounding was used to reduce the speckles in the sub-images for the attenuation coefficient estimation. In addition to the aforementioned simulation and experimental setups, a beef sample was positioned above the CIRS phantom, employing the same configuration as the previous experiments. The purpose of including the beef sample was to mimic the presence of a tissue-like structure in the imaging scenario. This additional element served to assess the performance and robustness of the proposed method in a more realistic setting and to evaluate the axial spatial resolution.

## III. RESULTS

### A. Comparison between DC and DAS in pressure amplitude and attenuation coefficient estimation

As a comparison with the DC method, the delay and sum (DAS) approach was first used to estimate the attenuation coefficient slope in the CIRS phantom of 0.7 dB/cm.MHz (Fig. 1). Fig. 1(a) shows the plots of the pressure amplitude vs. depth at three sub-bands in a ROI and the corresponding linear fittings to estimate the attenuation coefficients; Fig. 1(b) shows the plot of the attenuation coefficients vs. sub-band frequency and the corresponding linear fitting to estimate the attenuation coefficient slope. The ACS in Fig. 1(b) is 0.96 dB/cm.MHz, deviating from the actual value 0.7 dB/cm.MHz significantly.

In contrast, similar plots from the decorrelated compounding method are presented in Fig. 2 from a simulation phantom, the

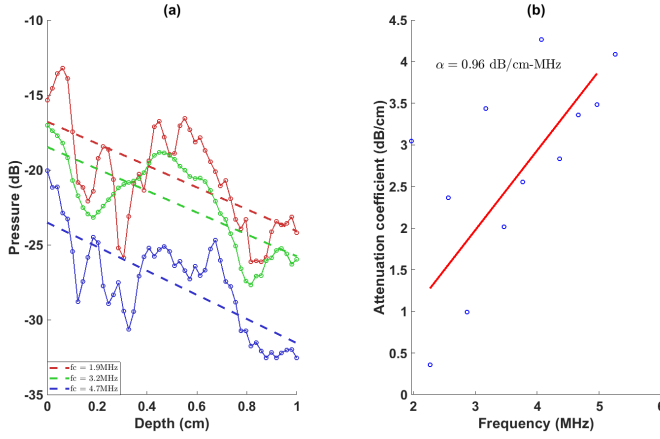


Fig. 1. (a) the plots of the pressure amplitude vs. depth at three sub-bands in an ROI in a CIRS phantom of 0.7 dB/cm.MHz and the corresponding linear fittings to estimate the attenuation coefficients; (b) the plot of the attenuation coefficients vs. sub-band frequency and the corresponding linear fitting to estimate the attenuation coefficient slope.

CIRS phantom, and the beef sample. The pressure amplitude plots in Fig. 2 show a much smaller than Fig. 1 due to the decorrelated compounding method, resulting in a more accurate estimation of the attenuation coefficient and ACS.

Figure 3 compares the ACS vs. depth plot using the DC method (blue) and delay and sum (DAS) approach (red). The DC approach provides much more stable estimates of the ACS along the depth than the DAS method.

### B. Simulation results

The average ACS values of five identical and independent simulated phantoms are plotted as a function of depth in Fig. 4. The standard deviation among the five phantoms is plotted as the error bar. In evaluating the accuracy of the attenuation coefficient slope, a relative error of up to 15% was considered acceptable [31].

### C. Tissue-mimicking experimental phantoms

To evaluate the ACS estimation performances quantitatively in tissue-mimicking experimental phantoms, we selected a uniform region of CIRS phantoms. Fig. 5 and Fig. 6 illustrate the plots of the estimated slope of attenuation coefficients versus depth for the CIRS phantom of 0.7 dB/cm.MHz and 0.5 dB/cm.MHz, respectively. The estimates of ACS obtained using the proposed method are consistently close to the actual values.

### D. Beef - Tissue-mimicking phantom analysis

Fig. 2(a) illustrate the plots of the estimated slope of attenuation coefficients versus depth for a composite sample with a piece of beef on top of the CIRS phantom of 0.7 dB/cm.MHz. The estimates of ACS in the CIRS phantom are again consistently close to the actual values. Fig. 2(a) can be considered as a n edge spread function because there is an interface between two different materials. The magnitude of the derivative of a edge spread function [Fig. 2(b)] gives a line

spread function, the FWHM of which can be used as a metric for spatial resolution along the axial direction.

In the beef sample part of Fig. 2(b), the average ACS was measured to be 1.1 dB/cm-MHz, which aligns with the literature-reported value [32, 33]. Similarly, in the phantom region, the average attenuation coefficient was determined to be 0.72 dB/cm-MHz, closely matching the expected value of 0.7 dB/cm-MHz. However, noticeable fluctuations in the attenuation values were observed at the interface region between the beef and the phantom. These variations can be attributed to the large specular reflection signals due to the acoustic impedance mismatch between the two materials. It should be noticed that the specular reflection signals have a different spectrum from the signal scattered from particles. Consequently, the spectrum-based method will not work with the specular reflection signals. In addition, the assumption of a uniform backscattering coefficient [ $BSC(f, z)$  in Eq. 1] inside the 1-cm ROI is violated at the beef-phantom interface due to the large specular reflection.

The axial resolution of the proposed method at the given configuration was estimated to be 0.7 cm through the full-width-at-half-maximum (FWHM) of the line spread function (LSF) (Fig. 7 (c)). Consequently, the proposed method successfully discriminates between the two regions, namely the beef sample and the phantom, enabling reliable differentiation based on their distinct attenuation characteristics.

## IV. DISCUSSION

### A. Additional comments on the results

It should be pointed out that the attenuation coefficient estimated from the experimental data is not the true value, but has a constant difference from the true value for each plot of attenuation coefficient vs. frequency. This is because there was a time-gated compensation (TGC) from ultrasound scanners. However, this TGC depends only on the depth, not on the signal frequency. Therefore, the effect of TGC will be a constant shift of the attenuation coefficient for all frequencies. That's why TGC will not affect the estimation of ACS. However, when comparing Fig. 2 (b) and (d), we can find that the attenuation coefficient in b is slightly larger than (d) at the same frequency. This is probably due to the TGC in experiments, which is lacking in simulation studies. TGC usually amplifies the signal at a larger depth more strongly. Therefore, TGC will make the attenuation coefficient appear smaller, as shown by our results. Nevertheless, TGC information is usually available. Therefore, we can remove the effect of TGC on the attenuation estimation and produce the true attenuation coefficient of tissues on top of the ACS.

It can be noticed that the ACS from the location very close to the probe (depth  $< 1.5\text{cm}$ ) in Fig. 4 and 5 gradually increases to the true value. This might be due to the oblique path from the probe elements to the imaged point when the image pixel location is close to the probe. When we use the derivative of pressure amplitude over depth to estimate the attenuation coefficient, the results will be smaller than the truth. Similar to the well-known fact that there is a natural focus due to the diffraction effect at the near-field



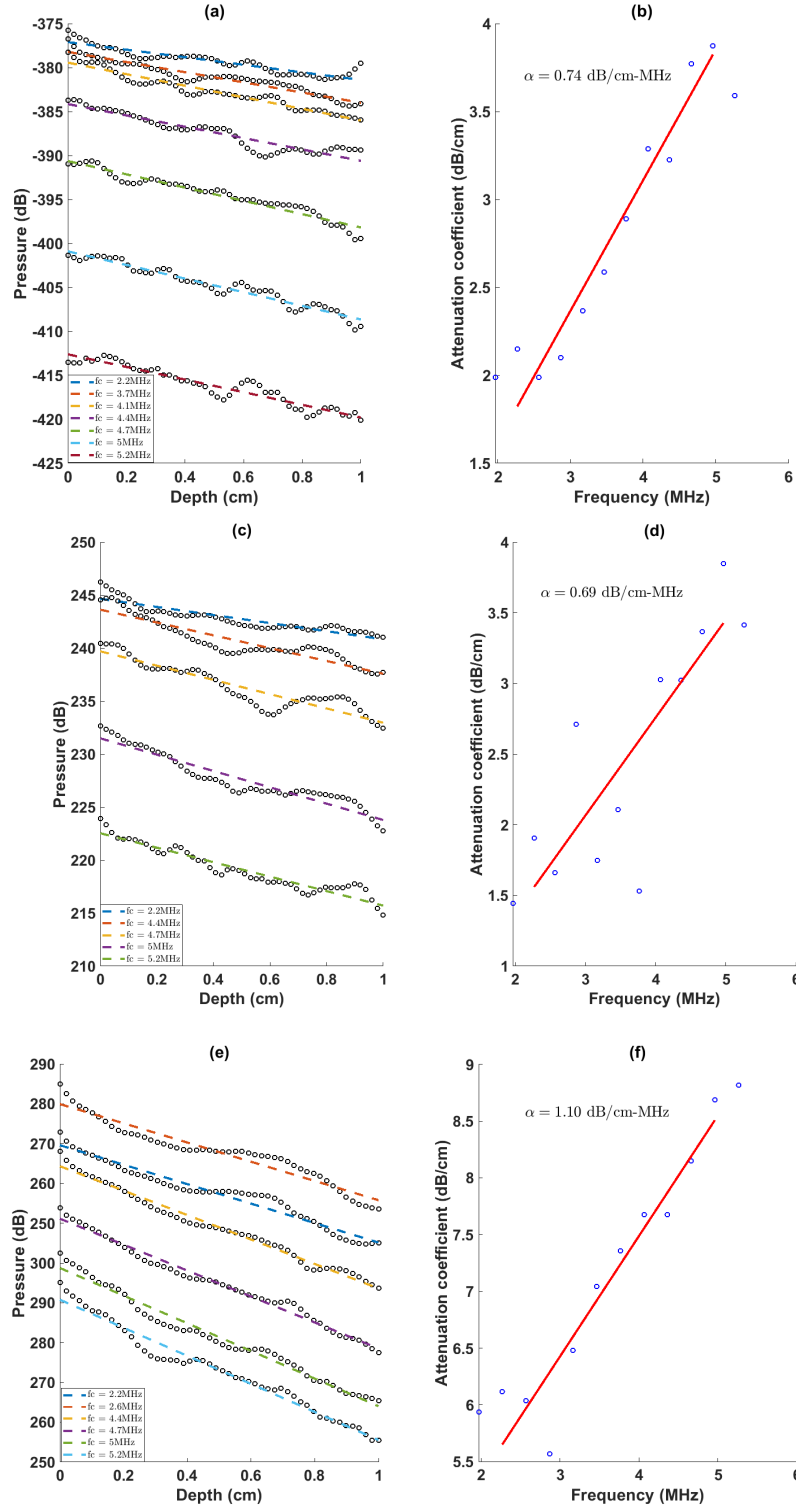


**Fig. 2.** (a), (c), and (e) are the plots of the pressure amplitude vs. depth at various sub-bands in an ROI in a simulation phantom, a CIRS phantom of 0.7 dB/cm.MHz phantom, and a beef phantom, respectively. (b), (d), and (f) are the corresponding plots of the attenuation coefficients vs. sub-band frequency and the corresponding linear fitting to estimate the attenuation coefficient slope in a simulation phantom, a CIRS phantom of 0.7 dB/cm.MHz phantom, and a beef phantom, respectively.

boundary of an unfocused transducer, there might be a pressure amplitude peak in STA images around 3 cm depth for the given parameters in our study. A weak focus can result in a decrease in the estimated attenuation coefficient.

In Fig. 4, there is a dip of ACS at 3 cm depth. Since the

results are the average of five identical independent phantoms, the dip should not be caused by medium fluctuation. We suspect the dip is due to some minor diffraction effect.

The decorrelated compounding technique has brought notable improvements in the image signal-to-noise ratio (SNR)

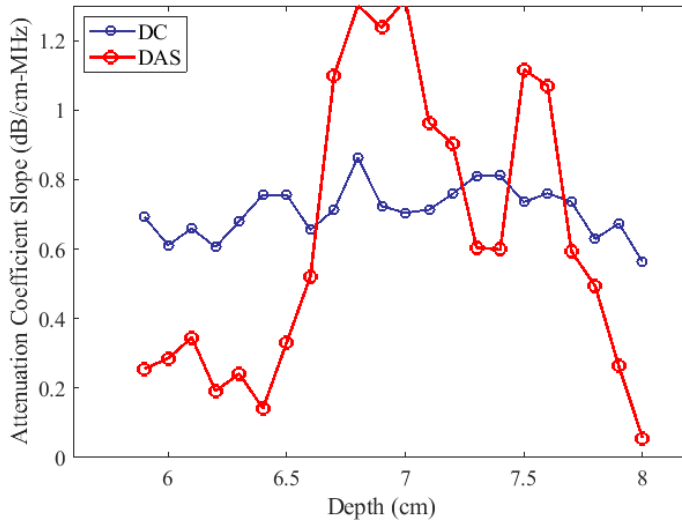


Fig. 3. Comparison of the ACS vs. depth plot using the DC method (blue) and delay and sum (DAS) approach (red) in a CIRS phantom of 0.7 dB/cm.MHz

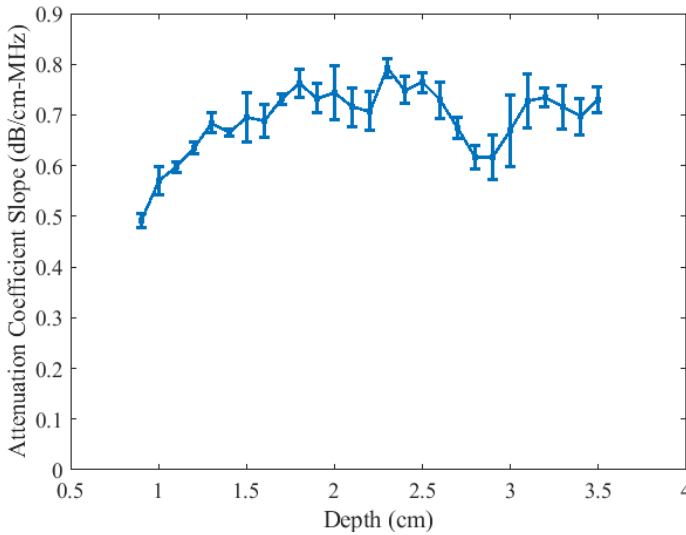


Fig. 4. The average attenuation coefficient slope( $\alpha$ ) and the standard deviation determined at different depths from five identical and independent simulated 0.7 dB/cm.MHz phantoms.

for both simulated and experimental images. Generally, there is a trade-off between the spatial resolution and the estimation accuracy in quantitative ultrasound. This enhanced SNR, as achieved by our method, is pivotal as it directly translates to more accurate and reliable estimations of attenuation coefficients. In the future, we can explore the feasibility of reducing the window size with parametric regularization [20] to improve spatial resolution.

Another benefit of using STA is the large range of depth of imaging ACS. As shown in Fig. 4 and 5 ACS can be imaged reasonably well from around 1-cm depth to 8-cm depth from one frame of image data. This is possible because optimum focusing can be achieved at all points in STA images and the diffraction effect is minimum in STA. Since the proposed method needs no reference phantom due to the minimum diffraction effect, its translation to clinical application should

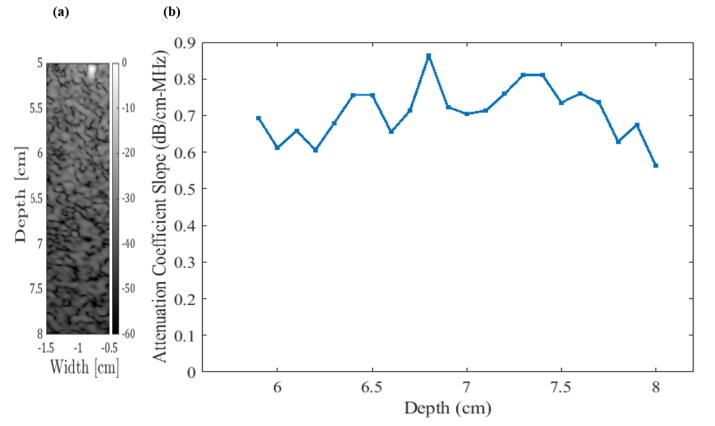


Fig. 5. a) Image illustrating the selected ROI in the CIRS phantom of 0.7 dB/cm.MHz. b) estimation of attenuation coefficient slope along the depth in the CIRS phantom

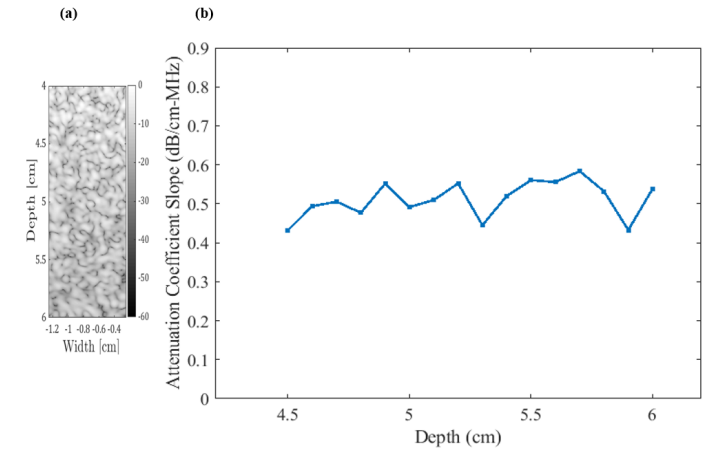


Fig. 6. a) Image illustrating the selected ROI in the CIRS phantom of 0.5 dB/cm.MHz. b) estimation of attenuation coefficient slope along the depth in the CIRS phantom.

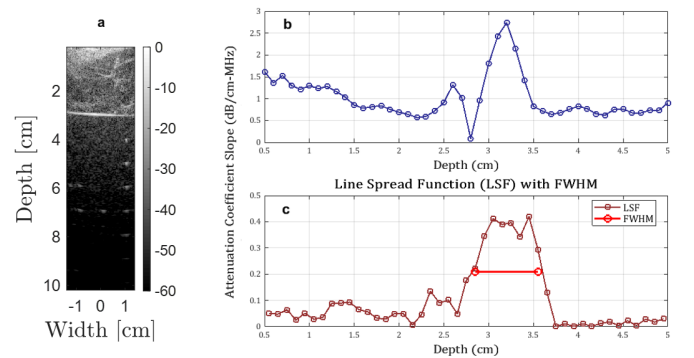


Fig. 7. a) Image illustrating the selected ROI in the composite sample with a piece of beef on top of the CIRS phantom of 0.7 dB/cm.MHz; b) the plot of the estimated slope of attenuation coefficients versus depth; c) the magnitude of the derivative of (b) as an approximation to the line spread function .

be easier than the reference-phantom method.

One advantage of the proposed method is that it first estimates the attenuation coefficient, and then the attenuation coefficient slope. There is no assumption of linear frequency

dependence of the attenuation coefficient, as in other methods. Since it is known that the attenuation coefficient of many tissues depends on the frequency in a nonlinear way, this advantage can provide further information for diagnosis by using attenuation coefficient as a bio-marker.

### B. Challenges to be addressed in future studies

The observed fluctuations in the attenuation values at the interface region between the beef sample and the tissue-mimicking phantom (Fig. 7) can be attributed to several factors. Previous studies have reported similar fluctuations involving interface regions between different materials [26, 34]. It's imperative to note that such interfaces inherently present challenges in consistent estimations. These fluctuations can arise due to the differences in the acoustic properties and scattering characteristics of the two materials, resulting in variations in the attenuation values along the interface. Additionally, the presence of interfaces can lead to partial reflection and refraction of the ultrasound waves, causing interference patterns and resulting in attenuation variations [35]. One approach to handle this challenge is to estimate the attenuation and tissue backscattering coefficients simultaneously, as shown in B-mode in [26]. We plan to explore this approach in STA in the future study.

The goal of this paper is to demonstrate the feasibility of the proposed method. There are still many parameters to be optimized for improved image quality. For example, the ROI size, the linear fitting methods, and the decorrelated compounding parameters (sub-aperture size, sub-band width, and the corresponding step sizes). Additionally, we will investigate reducing the computation load of the method so that it can be used for clinical investigations. A comparison between the current B-mode methods (spectral-based methods) [20] and the proposed STA method will be made.

Although the proposed method is based on STA data, it can be easily extended to B-mode data. The best option is to recover STA data from the pre-beamformed B-mode channel data through the decoding process with regularization [36, 37]. Then the proposed method can be applied to the recovered STA data. As discussed before, there is some information loss in this recovery process. Therefore, it will be an interesting future study to investigate how this decoding process will affect the performance of the proposed method. In clinics, harmonic imaging is very common because of the ability to suppress the aberration. Harmonic imaging can only be done in B-mode, not in STA mode. Therefore it is desirable to be able to extend our method to B-mode data.

## V. CONCLUSION

In conclusion, we proposed to apply decorrelated compounding method to estimating the attenuation coefficient in STA. The attenuation measurements obtained using the synthetic aperture technique in the simulations of the tissue-mimicking phantom and the analysis of the beef phantom highlight the effectiveness of this approach for estimating the attenuation coefficient. The synthetic aperture technique offers

benefits over traditional B-mode imaging in terms of accurate quantification of tissue properties. Further research and comparative studies are warranted to validate the findings and explore the full potential of the synthetic aperture technique in clinical applications.

## ACKNOWLEDGMENT

The authors would like to thank the following funding agencies: Natural Sciences and Engineering Research Council of Canada (NSERC), Canada Foundation for Innovation (CFI), and Toronto Metropolitan University.

## REFERENCES

- [1] G. Cloutier, F. Destrempes, F. Yu, and A. Tang, "Quantitative ultrasound imaging of soft biological tissues: A primer for radiologists and medical physicists," *Insights into Imaging*, vol. 12, pp. 1–20, 2021.
- [2] A. Coila, J. Rouyer, O. Zenteno, A. Luchies, M. L. Oelze, and R. Lavarello, "Total attenuation compensation for backscatter coefficient estimation using full angular spatial compounding," *Ultrasonics*, vol. 114, p. 106376, 2021.
- [3] D. Jesper *et al.*, "Ultrasound-based attenuation imaging for the non-invasive quantification of liver fat—a pilot study on feasibility and inter-observer variability," *IEEE Journal of Translational Engineering in Health and Medicine*, vol. 8, pp. 1–9, 2020.
- [4] K. Prabusankarlal, P. Thirumoorthy, and R. Manavalan, "Computer aided breast cancer diagnosis techniques in ultrasound: A survey," *Journal of Medical Imaging and Health Informatics*, vol. 4, no. 3, pp. 331–349, 2014.
- [5] K. H. Song and L. V. Wang, "Noninvasive photoacoustic imaging of the thoracic cavity and the kidney in small and large animals," *Medical physics*, vol. 35, no. 10, pp. 4524–4529, 2008.
- [6] E. J. Feleppa, J. Mamou, C. R. Porter, and J. Machi, "Quantitative ultrasound in cancer imaging," in *Seminars in oncology*, Elsevier, vol. 38, 2011, pp. 136–150.
- [7] M. L. Oelze and J. Mamou, "Review of quantitative ultrasound: Envelope statistics and backscatter coefficient imaging and contributions to diagnostic ultrasound," *IEEE Transactions on Ultrasonics, Ferroelectrics, and Frequency Control*, vol. 63, pp. 336–351, 2 Feb. 2016, ISSN: 08853010.
- [8] Y. Labyed and T. A. Bigelow, "A theoretical comparison of attenuation measurement techniques from backscattered ultrasound echoes," *The Journal of the Acoustical Society of America*, vol. 129, no. 4, pp. 2316–2324, 2011.
- [9] K. Samimi and T. Varghese, "Performance evaluation of the spectral centroid downshift method for attenuation estimation," *IEEE transactions on ultrasonics, ferroelectrics, and frequency control*, vol. 62, no. 5, pp. 871–880, 2015.

- [10] L. X. Yao, J. A. Zagzebski, and E. L. Madsen, "Backscatter coefficient measurements using a reference phantom to extract depth-dependent instrumentation factors," *Ultrasonic imaging*, vol. 12, no. 1, pp. 58–70, 1990.
- [11] L. Castañeda-Martinez, H. Rivaz, and I. Rosado-Mendez, "Comparison of different attenuation compensation methods in the estimation of the ultrasound backscatter coefficient," in *AIP Conference Proceedings*, AIP Publishing, vol. 2348, 2021.
- [12] A. L. Coila and R. Lavarello, "Regularized spectral log difference technique for ultrasonic attenuation imaging," *IEEE transactions on ultrasonics, ferroelectrics, and frequency control*, vol. 65, no. 3, pp. 378–389, 2017.
- [13] Z. Vajihi, I. M. Rosado-Mendez, T. J. Hall, and H. Rivaz, "Low variance estimation of backscatter quantitative ultrasound parameters using dynamic programming," *IEEE transactions on ultrasonics, ferroelectrics, and frequency control*, vol. 65, no. 11, pp. 2042–2053, 2018.
- [14] R. Rau, O. Unal, D. Schweizer, V. Vishnevskiy, and O. Goksel, "Frequency-dependent attenuation reconstruction with an acoustic reflector," *Medical Image Analysis*, vol. 67, p. 101875, 2021.
- [15] H. Tu, T. Varghese, E. L. Madsen, Q. Chen, and J. A. Zagzebski, "Ultrasound attenuation imaging using compound acquisition and processing," *Ultrasonic imaging*, vol. 25, no. 4, pp. 245–261, 2003.
- [16] J. M. Thijssen, "Ultrasonic speckle formation, analysis and processing applied to tissue characterization," *Pattern Recognition Letters*, vol. 24, no. 4-5, pp. 659–675, 2003.
- [17] N. Rubert and T. Varghese, "Scatterer number density considerations in reference phantom-based attenuation estimation," *Ultrasound in medicine & biology*, vol. 40, no. 7, pp. 1680–1696, 2014.
- [18] M. L. Oelze and J. Mamou, "Review of quantitative ultrasound: Envelope statistics and backscatter coefficient imaging and contributions to diagnostic ultrasound," *IEEE transactions on ultrasonics, ferroelectrics, and frequency control*, vol. 63, no. 2, pp. 336–351, 2016.
- [19] P. Gong, P. Song, C. Huang, J. Trzasko, and S. Chen, "System-independent ultrasound attenuation coefficient estimation using spectra normalization," *IEEE transactions on ultrasonics, ferroelectrics, and frequency control*, vol. 66, no. 5, pp. 867–875, 2019.
- [20] I. Rafati, F. Destrepes, L. Yazdani, M. Gesnik, A. Tang, and G. Cloutier, "Regularized ultrasound phantom-free local attenuation coefficient slope (acs) imaging in homogeneous and heterogeneous tissues," *IEEE Transactions on Ultrasonics, Ferroelectrics, and Frequency Control*, vol. 69, no. 12, pp. 3338–3352, 2022.
- [21] S. Dange, "Synthetic aperture ultrasound imaging a review," in *2020 IEEE 4th Conference on Information & Communication Technology (CICT)*, IEEE, 2020, pp. 1–6.
- [22] N. Zhao and Y. Xu, "Decorrelated compounding improves lesion signal-to-noise ratio of low-contrast lesions in synthetic transmit aperture ultrasound imaging," *JASA Express Letters*, vol. 2, no. 2, 2022.
- [23] N. Bottenus, M. LeFevre, J. Cleve, A. L. Crowley, and G. Trahey, "Resolution and speckle reduction in cardiac imaging," *IEEE transactions on ultrasonics, ferroelectrics, and frequency control*, vol. 68, no. 4, pp. 1131–1143, 2020.
- [24] G. Chau, M. Jakovljevic, R. Lavarello, and J. Dahl, "A locally adaptive phase aberration correction (lapac) method for synthetic aperture sequences," *Ultrasonic imaging*, vol. 41, no. 1, pp. 3–16, 2019.
- [25] N. Zhao and Y. Xu, "Decorrelated compounding in synthetic transmit aperture (sta) ultrasound imaging to detect low-contrast lesions," in *2020 IEEE International Ultrasonics Symposium (IUS)*, IEEE, 2020, pp. 1–4.
- [26] K. Nam, J. A. Zagzebski, and T. J. Hall, "Simultaneous backscatter and attenuation estimation using a least squares method with constraints," *Ultrasound in medicine & biology*, vol. 37, no. 12, pp. 2096–2104, 2011.
- [27] K. A. Wear, "A gaussian framework for modeling effects of frequency-dependent attenuation, frequency-dependent scattering, and gating," *IEEE transactions on ultrasonics, ferroelectrics, and frequency control*, vol. 49, no. 11, pp. 1572–1582, 2002.
- [28] K. Nam, I. M. Rosado-Mendez, N. C. Rubert, E. L. Madsen, J. A. Zagzebski, and T. J. Hall, "Ultrasound attenuation measurements using a reference phantom with sound speed mismatch," *Ultrasonic imaging*, vol. 33, no. 4, pp. 251–263, 2011.
- [29] N. Zhao and Y. Xu, "Decorrelated compounding improves lesion signal-to-noise ratio of low-contrast lesions in synthetic transmit aperture ultrasound imaging," *JASA Express Letters*, vol. 2, no. 2, p. 022001, 2022.
- [30] J. A. Jensen, "Field: A program for simulating ultrasound systems," *Medical & Biological Engineering & Computing*, vol. 34, no. sup. 1, pp. 351–353, 1997.
- [31] N. Ilyina, J. Hermans, E. Verboven, K. Van Den Abeele, E. D'Agostino, and J. D'hooge, "Attenuation estimation by repeatedly solving the forward scattering problem," *Ultrasonics*, vol. 84, pp. 201–209, 2018.
- [32] R. Xu, B. E. Treeby, and E. Martin, "Experiments and simulations demonstrating the rapid ultrasonic re-warming of frozen tissue cryovials," *The Journal of the Acoustical Society of America*, vol. 153, no. 1, pp. 517–528, 2023.
- [33] D. Shore, M. Woods, and C. Miles, "Attenuation of ultrasound in post rigor bovine skeletal muscle," *Ultrasonics*, vol. 24, no. 2, pp. 81–87, 1986.
- [34] H. Kim and T. Varghese, "Hybrid spectral domain method for attenuation slope estimation," *Ultrasound in medicine & biology*, vol. 34, no. 11, pp. 1808–1819, 2008.
- [35] F. M. Hooi, O. Kripfgans, and P. L. Carson, "Acoustic attenuation imaging of tissue bulk properties with a pri-



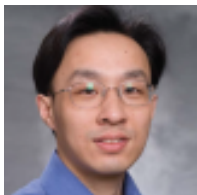
ori information,” *The Journal of the Acoustical Society of America*, vol. 140, no. 3, pp. 2113–2122, 2016.

- [36] P. Gong, M. C. Kolios, and Y. Xu, “Delay-encoded transmission and image reconstruction method in synthetic transmit aperture imaging,” *IEEE Transactions on Ultrasonics, Ferroelectrics, and Frequency Control*, vol. 62, no. 10, pp. 1745–1756, 2015, ISSN: 0885-3010.
- [37] N. Bottenus, “Recovery of the complete data set from focused transmit beams,” *IEEE Transactions on Ultrasonics, Ferroelectrics, and Frequency Control*, vol. 65, pp. 30–38, 1 Jan. 2018, ISSN: 08853010.



**Khalid Abdalla** received his B.Sc. degree in Physics from Mut’ah University, Jordan, and went on to achieve an M.Sc. in Medical Physics from King Fahd University, KSA, in 2006. His pioneering research during this period focused on boron neutron capture therapy. In 2019, he earned another M.Sc. degree in Medical Biophysics from Western University, London, Canada. At Western, he embarked on an in-depth study of myocardial R2\* mapping pre- and post-myocardial infarction in canine models,

a significant research endeavor for which he was honored with the Western Graduate Research Scholarship. Khalid is currently pursuing his Ph.D. in Biomedical Physics at Toronto Metropolitan University, specializing in the acoustic attenuation coefficient in synthetic aperture ultrasound imaging.



**Yuan Xu** was born in China, in 1971. He received the Ph.D. degree in physics from the Institute of Physics, Chinese Academy of Sciences, Beijing, China, in 1999, and the Ph.D. degree in biomedical engineering from Texas A&M University, College Station, TX, USA, in 2003. Since 2005, he has been working with Ryerson University, Toronto, ON, Canada, where he is currently a Professor with the Department of Physics. His research interests include the development of novel algorithms to improve the

image qualities of ultrasound images and to reduce the cost of ultrasound imaging systems.